Published in final edited form as:

J Phys Chem Lett. 2023 January 12; 14(1): 95–100. doi:10.1021/acs.jpclett.2c03087.

Amplified Overhauser DNP with Selective Deuteration: Attenuation of Double-Quantum Cross-Relaxation

Ravi Shankar Palani[¶],
Department of Chemistry and Francis Bitter Magnet Laboratory, Massachusetts Institute of Technology, Cambridge, Massachusetts 02139, United States

Michael Mardini[¶],
Department of Chemistry and Francis Bitter Magnet Laboratory, Massachusetts Institute of Technology, Cambridge, Massachusetts 02139, United States

Leo Delage-Laurin,
Department of Chemistry and Institute for Soldier Nanotechnologies, Massachusetts Institute of Technology, Cambridge, Massachusetts 02139, United States

Daniel Banks,
Bruker Biospin Corporation, Billerica, Massachusetts 01821, United States

Yifu Ouyang,
Department of Chemistry and Francis Bitter Magnet Laboratory, Massachusetts Institute of Technology, Cambridge, Massachusetts 02139, United States

Eric Bryerton,
Virginia Diodes Corporation, Charlottesville, Virginia 22902, United States

James G. Kempf,
Bruker Biospin Corporation, Billerica, Massachusetts 01821, United States

Timothy M. Swager,
Department of Chemistry, Massachusetts Institute of Technology, Cambridge, Massachusetts 02139, United States

Robert G. Griffin
Department of Chemistry and Francis Bitter Magnet Laboratory, Massachusetts Institute of Technology, Cambridge, Massachusetts 02139, United States

Abstract

Corresponding Author: **Robert G. Griffin** – Department of Chemistry and Francis Bitter Magnet Laboratory, Massachusetts Institute of Technology, Cambridge, Massachusetts 02139, United States; rgg@mit.edu.
[¶]R.S.P. and M.M. contributed equally to the work

Complete contact information is available at: https://pubs.acs.org/10.1021/acs.jpclett.2c03087

Supporting Information
The Supporting Information is available free of charge at https://pubs.acs.org/doi/10.1021/acs.jpclett.2c03087.
Details of synthesis, ^{1}H and ^{13}C spectra of intermediates in the synthesis, and UV–vis spectra of DNP samples (PDF)

The authors declare no competing financial interest.

We recently used selective ^{2}H labeling of BDPA to investigate the Overhauser Effect (OE) dynamic nuclear polarization (DNP) mechanism in insulating solids doped with 1,3-bis(diphenylene)-2-phenylallyl (BDPA), and established that the α and γ ^{1}H spins on the fluorene rings are responsible for generating a zero quantum (ZQ) mediated *positive* bulk polarization. Here, we establish that the phenyl ^{1}H spins relax via double-quantum (DQ) processes and therefore contribute *negative* enhancements which attenuate the OE-DNP. With measurements at different magnetic field strengths, we show that phenyl-d_5-BDPA offers >50% improvement in OE-DNP enhancement compared to h_{21}-BDPA attaining a maximum of ~ 90 at 14.1 T and 5 kHz MAS, the highest observed OE-DNP enhancement to date under these conditions. The approach may be utilized to optimize other polarizing agents exhibiting an OE, an important DNP mechanism with a favorable field and spinning frequency dependence.

Graphical Abstract

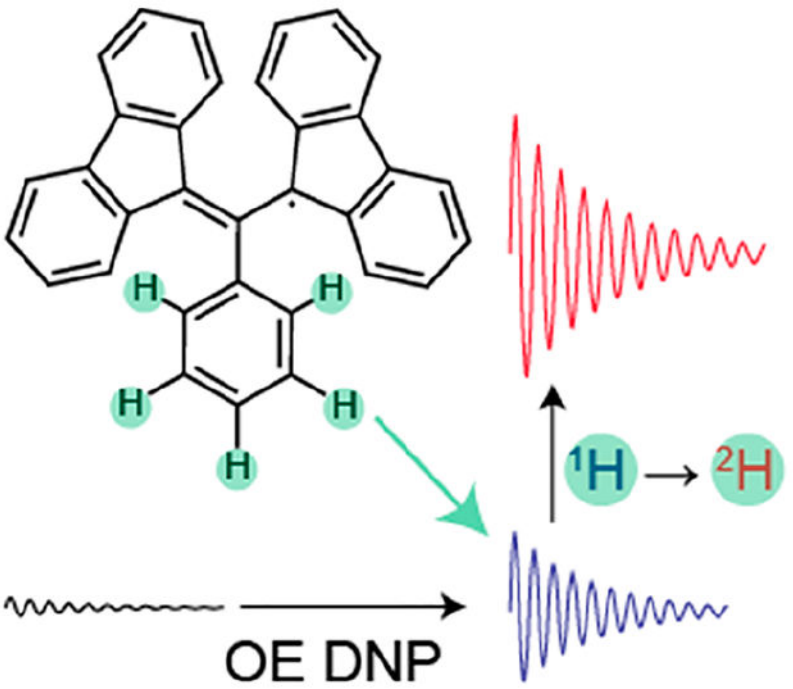

Nuclear magnetic resonance (NMR) spectroscopy suffers from low sensitivity due to the small size of the nuclear spin energy splittings relative to the thermal energy. Dynamic nuclear polarization (DNP) overcomes this difficulty by using microwave irradiation of electron–nuclear transitions to transfer the polarization of electron spins to the nuclei of interest.[1–3] The increased sensitivity available from DNP has revolutionized the field of NMR, both in liquids and solids, and has enabled the structural studies[4,5] of biomolecules and materials in more complex environments than were previously feasible.[6–11]

Particularly effective approaches to DNP rely on coherent manipulation of the electron spin polarization and require that the electron Rabi frequency, ω_{1e}, be greater than the spin–spin relaxation rate of the electrons, $1/T_{2e}$, where T_{2e}, the electron transverse relaxation time,

is typically on the order of a few microseconds. ω_{1e} is proportional to the square root of microwave power, and with current technology, this usually ranges from a few milliwatts to tens of watts. Although higher powers have been achieved,[12] microwave power is a limitation frequently encountered at magnetic field strengths exceeding 5 T.[13] Thus, absent a resonance microwave structure to boost efficiency in coupling ω_{1e} to the sample, the electron Rabi frequency is low and coherent transfers are presently not practical. However, the achievable Rabi fields are sufficient to support continuous-wave DNP (CW-DNP) mechanisms.[14,15] Accordingly, four known CW-DNP mechanisms are typically utilized in DNP experiments on solids: the solid effect (SE),[16,17] the cross effect (CE),[18–20] thermal mixing (TM),[21–24] and the Overhauser effect (OE).[2,25] Detailed discussions of the first three mechanisms–the SE, CE, and TM–are available in review articles[14,15,26]

The OE, which is the subject of this paper, requires coupled electron–nuclear spin pairs. Microwave irradiation at the EPR (electron paramagnetic resonance) frequency of a polarizing agent with a narrow line, such as BDPA, drives allowed single-quantum EPR transitions. Subsequent cross-relaxation in the coupled electron–nuclear spin system via zero quantum (ZQ) and double quantum (DQ) pathways with unequal rates results in enhanced polarization of the nuclear spins. The polarization buildup of the nuclear spins can be positive or negative, depending on whether either the ZQ or the DQ cross-relaxation is dominant, respectively. The advantages of the OE mechanism are that it scales positively with magnetic field and with increasing spinning frequency. Furthermore, because the EPR spectrum of BDPA is narrow, level crossing does not occur during spinning, and therefore, the OE is not subject to depolarization as is the CE.

The OE is usually observed in liquids, conducting solids, or doped semiconductors,[27,28] systems where there is mobility of the spins involved, i.e., where translational fluctuations drive cross-relaxation needed for DNP. More recently, OE DNP was surprisingly observed in insulating solids doped with BDPA.[29–33] Cross-relaxation requires time-dependent modulation of the hyperfine couplings, and the source of the modulation in insulating solids is yet to be definitively established. Recently, it was proposed that intramolecular charge transfer by the mixed-valence nature of BDPA could be responsible for the modulation[34] and other mixed-valence polarizing agents that exhibit the OE were recently reported.[32,35] It was also recently suggested that what is generally identified as an OE in BDPA is in fact due to TM;[36] however, this topic, while extremely interesting, is not the subject of research results presented here.

The primary topic explored here is the role of the ^{1}H nuclei on the polarization agent in facilitating DNP, and ultimately contributing to the diffusive spread of polarization throughout the sample. In a previous study, we investigated this role via the proton spins on the fluorene moieties (Scheme 1, top left) in determining OE DNP enhancements using selectively deuterated BDPA variants as the agent.[37] We established that the strongly coupled (~5.4 MHz) ^{1}H spins at the α and γ positions of the fluorenes are essential for generating positive enhancements, while the weakly coupled (~1 MHz) ^{1}H spins on the β and δ positions are likely crucial for efficient spin diffusion of the polarization from the ^{1}H spins on the radical to the bulk. We also observed a *negative* DNP enhancement of the bulk ^{1}H spins for 1,3-[d_{16}]-BDPA, where all the 16 ^{1}H positions in the fluorenes

were deuterated. This suggested that the ^{1}H spins on the phenyl ring, which exhibit small hyperfine couplings and have heretofore been considered *inconsequential*, cumulatively contributed to the negative enhancement observed in the bulk. However, their relative contributions to the OE DNP were unknown.

In this study, we determine the relative contributions of the ^{1}H spins on the phenyl ring and the ^{1}H spins in immediately surrounding *o*TP molecules to the overall negative polarization observed in the bulk ^{1}H spins. This was addressed by performing DNP experiments on a fully deuterated sample, and the data suggested that the ^{1}H spins on the phenyl ring and ^{1}H spins in the nearby *o*TP molecules were negatively polarized via a DQ OE DNP mechanism. Based on this, we used minimal chemistry to synthesize a phenyl-deuterated BDPA radical hypothesizing that it would result in improved positive OE DNP enhancement observed in the bulk. We verified this to be the case with DNP experiments performed at magnetic fields ranging from 5 to 14.1 T. Furthermore, we confirm that OE enhancements do scale with B_0 and that there is no depolarization because of the narrow line width of the BDPA EPR spectrum. For these reasons, it is important to develop further examples of OE radicals for use in DNP MAS experiments at high fields.

SYNTHESIS

Scheme 1 details the synthetic route used to synthesize Phe-d_5-BDPA, which is based on a previous report.[37] Synthetic routes to BDPA radicals are well established and Phe-d_5-BDPA can be obtained in four steps from readily available fluorene and benzaldehyde-d_6 or benzaldehyde-d_5. First, condensation of fluorene with one equivalent of benzaldehyde-d_5 delivered 9-((phenyl-d_5)methylene)-9H-fluorene (**1**) in 75% yield. Compound **1** was subsequently subjected to a two-step process consisting of an alkene bromination with bromine followed by dehydrobromination to obtain 9-(bromo(phenyl-d_5)-methylene)-9*H*-fluorene (**2**) in 59% yield. Next, **2** was condensed with another equivalent of fluorene via a nucleophilic addition–elimination sequence to form the neutral precursor Phe-d_5-BDPA-H (**3**) in 62% yield. Finally, radical formation to obtain Phe-d_5-BDPA was performed by deprotonation of **3**, followed by one-electron oxidation of the resulting anion using silver nitrate. This last step was performed with an 80% yield. For further experimental details on the synthesis of Phe-d_5-BDPA radical, we refer the reader to the Supporting Information.

The DNP experiments were performed using four different NMR/DNP spectrometers operating at the following fields, ^{1}H frequencies, and microwave frequencies for $g = 2$ electrons: 5.0 T/211 MHz/140 GHz, 8.9 T/380 MHz/250 GHz, 9.4 T/400 MHz/263 GHz, and 14.1 T/600 MHz/395 GHz. The DNP experiments on the 8.9 T/380 MHz/250 GHz spectrometer were performed with microwave irradiation from a home-built 250 GHz gyrotron delivering ~5 W of output power, and a low-power 160 mW solid-state source from Virginia Diodes, Inc. (VDI) (Figure 2a). The low-power microwave system uses an arbitrary waveform generator (Keysight AWG M8190A) and an amplifier multiplier chain (VDI AMC 691) and is capable of producing microwaves over a frequency range of 8 GHz from 246–254 GHz. The details of this instrument will be discussed in detail in a future publication. The gyrotron source of this DNP spectrometer is capable of producing microwaves at 250.02 GHz, which is required to observe the OE DNP in the BDPA samples

studied here. The DNP experiments on the 9.4 T/400 MHz/263 GHz spectrometer were performed with microwaves from a 280 mW amplifier multiplier chain (VDI AMC 749). The DNP experiments on the 14.1 T/600 MHz/395 GHz spectrometer were performed with a 30 W gyrotron at a fixed frequency of 395.285 GHz. The NMR magnetic field is swept to obtain DNP Zeeman profiles with a gyrotron, while the microwave frequency is swept at a fixed field with the solid-state sources. All the experiments were performed at a MAS frequency of $\omega_r/2\pi$ = 5 kHz, except for the experiments on the 5 T spectrometer which was performed at a MAS frequency of $\omega_r/2\pi$ = 3.5 kHz. The temperature of the sample was 90 K (5 and 8.9 T) or 100 K (9.4 and 14.1 T).

The DNP samples were prepared by doping 2.5 wt % of the radical, h_{21}-BDPA, Phe-d_5-BDPA, or d_{21}-BDPA, all in 1:1 complex with benzene, into a mixture of 95/5 mol % d_{14}- and h_{14}-*ortho*-terphenyl (*o*TP).[38] In molar concentrations, this corresponds to ~60.0 mM of h_{21}-BDPA, ~ 59.4 mM of Phe-d_5-BDPA, and ~ 57.5 mM of d_{21}-BDPA. h_{21}-BDPA was purchased from Sigma-Aldrich, while the Phe-d_5-BDPA was synthesized as discussed above. The perdeuterated d_{21}-BDPA was prepared using procedures described previously.[37] The doped mixture was dissolved in $CDCl_3$ which was removed by evaporation under a vacuum. The resulting thin film was finely ground and packed in a 4 mm sapphire rotor for experiments on the 5 and 8.9 T DNP spectrometers or a 3.2 mm sapphire rotor for experiments on the 9.4 and 14.1 T DNP spectrometers. The 4 mm sapphire rotors were subsequently warmed in a sand bath maintained at 60 °C for 5 min to melt the oTP and then quenched in liquid nitrogen to generate a glassy matrix. Subsequently, the sample was inserted into the precooled probe. A similar melt–quench procedure was used for the 3.2 mm sapphire rotors; however, a heat gun was used in place of a sand bath.

The NMR experiments involved a train of saturation pulses on the ^{1}H channel with a Rabi frequency of $\omega_1/2\pi$ = 83 kHz and 3 μs (5 and 8.9 T), $\omega_1/2\pi$ = 152 kHz and 1.65 μs (9.4 T), and $\omega_1/2\pi$ = 100 kHz and 2.5 μs (14.1 T). In all experiments, the interpulse delay of the saturation pulses was 220 μs. The signal was acquired following a recovery period using a solid–echo sequence. The spin–lattice relaxation times T_1 and the DNP buildup times T_B were estimated by fitting mono-exponential buildup curves to the signal intensities with varying recovery periods. The DNP enhancement was determined using $\varepsilon = (I/I_0) - 1$, where I denotes the NMR signal intensity with the microwaves on and I_0 denotes the NMR signal intensity with no microwave irradiation, both obtained at a recovery period of $1.3\,T_1$ or $1.3\,T_B$, whichever is longer.

Figure 1 shows a superposition of the ^{1}H DNP Zeeman frequency profiles recorded as a function of microwave irradiation frequency for 1,3-[$\alpha,\beta,\gamma,\delta$-$d_{16}$]-BDPA (reproduced from ref 37) and d_{21}-BDPA, the latter newly recorded on the 8.9 T DNP spectrometer with the low-power (160 mW) solid-state source. The d_{21}-BDPA sample was degassed using the procedure employed for the 1,3-[$\alpha,\beta,\gamma,\delta$-$d_{16}$]-BDPA sample with the freeze–pump–thaw protocol reported in our previous study.[37] Deuteration of the fluorene moieties in 1,3-[$\alpha,\beta,\gamma,\delta$-$d_{16}$]-BDPA resulted in a negative OE enhancement of $\varepsilon = -13$. However, perdeuteration to yield d_{21}-BDPA resulted in a smaller negative OE enhancement $\varepsilon = -6.4$. These results indicate that the ^{1}H spins on the phenyl ring are polarized negatively due to dominance of DQ cross-relaxation mechanisms in the e-−^{1}H systems. The conclusion

led us to propose a version of BDPA with only the phenyl ring deuterated so as to quench its negative contributions to the DNP enhancement and obtain a larger positive DNP enhancement than with h_{21}-BDPA.

Figure 2 shows a series of DNP frequency/field profiles observed for nondegassed h_{21}-BDPA and Phe-d_5-BDPA on the 5 T DNP spectrometer (Figure 2a), the 8.9 T spectrometer (Figure 2b), the 9.4 T spectrometer (Figure 2c), and the 14.1 T spectrometer (Figure 2d). These data were recorded on nondegassed samples as the 5 and 8.9 T DNP spectrometers utilized a 4 mm rotor, while the 9.4 and 14.1 T spectrometers utilized a 3.2 mm rotor, for which the samples were transported to a remote lab for experiments, where degassing equipment was not available. The OE enhancements, defined by the intensity of the central peak in each profile, for h_{21}-BDPA and Phe-d_5-BDPA samples were respectively 29 and 64 on the 5 T spectrometer, 36 and 67 on the 8.9 T spectrometer (160 mW), 40 and 70 on the 9.4 T spectrometer, and 49 and 88 on the 14.1 T spectrometer. The results demonstrate that Phe-d_5-BDPA consistently exhibits a higher OE DNP enhancement than the h_{21}-BDPA, at least up to a field strength of 14.1 T.

Table 1 summarizes the ^{1}H spin–lattice relaxation times for the sample doped with 2.5 wt % h_{21}-BDPA and Phe-d_5-BDPA as measured at 8.9 and 14.1 T DNP spectrometers. Table 2 lists the enhancement values measured for the two radicals with an incident microwave power of 2 W at 5 T, with an incident microwave power of 160 mW at 8.9 T, and 4.4 W at 250.020 GHz, with an incident microwave power of 280 mW at 9.4 T and 264.250 GHz, and with an incident microwave power of 30 W at 14.1 T and 395.285 GHz. Using UV–vis absorption measurements, we determined the relative concentrations of active free radicals between the two samples, both prepared at 2.5 wt %, to be 1.0:1.2 for h_{21}-BDPA and Phe-d_5-BDPA, respectively (see Figure S8). The enhancement values adjusted for the relative concentrations are also listed in Table 2. This is done since the commercially available BDPA samples were not 100% active. We also note there is no evidence as yet for linear dependence of the enhancement on concentration.

Figure 3a shows the dependence of the measured DNP enhancement as a function of MAS frequency at the 9.4 T DNP spectrometer. The 3.2 mm sapphire rotor at about 100 K could only spin at a maximum of 12.5 kHz. Figure 3b shows the dependence of the measured DNP enhancement as a function of microwave irradiation power at the 9.4 T DNP spectrometer equipped with a solid-state microwave source with a maximum output power of 280 mW (filled circles). There are additional points (empty circles) in the plot showing the DNP enhancements with 4.4 W of irradiation power for the two polarizing agents obtained on the 8.9 T DNP spectrometer.

The OE ideally involves a two-spin system of one electron and one nucleus, hyperfine coupled to each other. The nucleus in our discussion is an ^{1}H spin–either on the BDPA molecule itself or on the surrounding oTP molecules. The excitation of the electron spin transition is followed by unequal cross-relaxation rates in the electron–nuclear two-spin system that can polarize the nuclear spin either positively or negatively. The sign depends on whether the dominant cross-relaxation mechanism is ZQ or DQ, respectively. Cross-relaxation requires time-modulation of the hyperfine coupling and the isotropic component

leads to ZQ cross-relaxation while the anisotropic component leads to DQ cross-relaxation. The observed NMR signal is that of the bulk ^{1}H spins in the oTP matrix after they equilibrate with the directly polarized ^{1}H spins in and immediately around the radical. Thus, the observed enhancement in the bulk nuclear spins results from the cumulative contribution of both positive and negative contributions originating in the ^{1}H spins coupled to the electron. In an earlier study, we used the DNP frequency profiles of selectively deuterated BDPA radicals to determine that the strongly coupled ^{1}H spins on the α,γ sites of the fluorene moieties generate a significant positive OE enhancement. In contrast, the weakly hyperfine coupled ^{1}H spins on the β,δ sites on the fluorene moieties primarily aid efficient spin diffusion of the enhanced polarization from the α,γ sites to the bulk ^{1}H spins in the matrix.

Figure 1 illustrates an OE enhancement of $\varepsilon = -13$ for 1,3-[$\alpha,\beta,\gamma,\delta$-$d_{16}$]-BDPA, which we reported in our earlier study.[37] This suggests that the ^{1}H spins on the phenyl ring and the oTP molecules in the surrounding matrix cumulatively make a negative contribution to the overall OE enhancement. However, the relative contributions between the ^{1}H spins on the phenyl ring and the surrounding oTP molecules to the overall negative DNP enhancement were unknown. To determine this, in this work, we measured the OE enhancement on d_{21}-BDPA and obtained an enhancement of $\varepsilon = -6.4$. The relative concentrations between the two samples–1,3-[$\alpha,\beta,\gamma,\delta$-$d_{16}$]-BDPA and d_{21}-BDPA–were determined using UV–vis spectroscopy to be 1.4:1.0, respectively, and this is attributed to the partial decay (reduction) of the radicals to different levels. Adjusting for the concentrations, the negative DNP enhancement of 1,3-[$\alpha,\beta,\gamma,\delta$-$d_{16}$]-BDPA was about 45% larger than the negative DNP enhancement obtained for d_{21}-BDPA. The result suggests that the ^{1}H spins on the phenyl ring of the BDPA radical and the ^{1}H spins on the surrounding oTP molecules were both individually polarized via a dominant DQ cross-relaxation mechanism in their respective electron–nuclear spin systems. That is, both groups of ^{1}H spins directly contribute to a negative enhancement. This finding leads us to propose that 2H labeling of the phenyl ring in the BDPA radical should lead to higher OE DNP enhancement than observed with the standard h_{21}-BDPA.

Our hypothesis is proven correct, as evidenced by DNP measurements performed in various DNP spectrometers and presented in Figure 2. For example, on the 8.9 T DNP spectrometer with the 160 mW microwave source, Phe-d_5- BDPA results in an OE enhancement of 67, in contrast to an enhancement of 36 observed for the standard h_{21}-BDPA. However, UV–vis measurements determined the relative radical concentration between h_{21}-BDPA and Phe-d_5-BDPA samples to be 1.0:1.2 (Figure S8). Adjusting for this, Phe-d_5-BDPA exhibits an OE enhancement ~ 52% higher than that of h_{21}-BDPA on the 8.9 T spectrometer. Similarly, the increase in enhancement is ~ 82%, ~ 48%, and ~ 50% on the 5, 9.4, and 14.1 T spectrometers, respectively.

Finally, we verified the dependence of the OE DNP enhancements on MAS frequency and microwave irradiation power for both radicals, as illustrated in Figure 3. The experiments were performed on the 9.4 T DNP spectrometer with the low-power microwave source and there is an additional data point in Figure 3B performed with 4.4 W microwave irradiation at the 8.9 T DNP spectrometer under otherwise similar experimental conditions. Both the

radicals exhibit increasing enhancement with increasing MAS frequency, while the power dependence appears to saturate with well under 1 W of microwave irradiation, consistent with prior investigations of OE DNP in insulating solids.[30,32,39] This is also encouraging for use of compact, lower-cost, low-power solid-state microwave sources.

Based on prior DNP data on selectively deuterated BDPA radicals and newly obtained data on a perdeuterated BDPA radical, we concluded that the ^{1}H spins on the phenyl ring of the BDPA radical participate in OE DNP primarily through DQ cross-relaxation, contributing a negative enhancement. We demonstrated that deuteration of the phenyl ring in the BDPA radical improves the overall positive OE enhancement compared to the standard h_{21}-BDPA by removing contributions to DQ cross-relaxation. We verified the hypothesis by synthesizing the newly proposed Phe-d_5-BDPA radical and examining its DNP properties in several spectrometers. In the magnetic field range of 5–14.1 T, the Phe-d_5-BDPA polarizing agent improves the OE DNP enhancement by about 50% when adjusted for the concentrations of active radicals in the sample, compared to the standard h_{21}-BDPA in the *o*TP matrix, and has achieved a maximum enhancement of ~ 90 at 14.1 T at a MAS frequency of 5 kHz at 100 K–the highest OE at these conditions to date for a nondegassed sample–and is expected to improve further by ~ 70% with freeze–pump–thaw degassing as demonstrated in our earlier study.[37] These results offer insight into designing new or modifying existing polarizing agents to exhibit amplified OE DNP. Considering the improvement of OE with stronger magnetic field strengths as shown here, in stark contrast to other CW-DNP mechanisms, the results discussed are of prime importance to achieve efficient sensitivity enhancements in high-resolution solid-state NMR of biological macromolecules. The work presented here also underscores the rationale for pursuing low-power solid-state microwave sources for use at high magnetic field strengths.

Supplementary Material

Refer to Web version on PubMed Central for supplementary material.

ACKNOWLEDGMENTS

This research was supported by grants to R.G.G. from the National Institutes of Health (GM-132997, AG-058504, and GM-132079) and to T.M.S. from the Air Force Office of Scientific Research (17RT0904; FA9550-18-1-0341)

REFERENCES

(1). Abragam A The Principles of Nuclear Magnetism; Clarendon: 1961.

(2). Overhauser AW Polarization of nuclei in metals. Phys. Rev 1953, 92 (2), 411.

(3). Slichter CP Principles of Magnetic Resonance; Springer-Verlag: 1989.

(4). Griffiths JM; Griffin RG Nuclear-Magnetic-Resonance Methods for Measuring Dipolar Couplings in Rotating Solids. Anal. Chim. Acta 1993, 283 (3), 1081–1101.

(5). Bennett AE; Griffin RG; Vega S Recoupling of Homo- and Heteronuclear Dipolar Interactions in Rotating Solids. NMR Basic Principles and Progress 1994, 33, 1–77.

(6). Hall DA; Maus DC; Gerfen GJ; Inati SJ; Becerra LR; Dahlquist FW; Griffin RG Polarization-enhanced NMR spectroscopy of biomolecules in frozen solution. Science 1997, 276 (5314), 930–932. [PubMed: 9139651]

(7). Bahri S; Silvers R; Michael B; Jaudzems K; Lalli D; Casano G; Ouari O; Lesage A; Pintacuda G; Linse S; et al. 1H detection and dynamic nuclear polarization-enhanced NMR of Aβ1–42 fibrils. Proc. Natl. Acad. Sci. U. S. A 2022, 119 (1), e2114413119. [PubMed: 34969859]

(8). Koers EJ; van der Cruijsen EA; Rosay M; Weingarth M; Prokofyev A; Sauvée C; Ouari O; van der Zwan J; Pongs O; Tordo P; et al. NMR-based structural biology enhanced by dynamic nuclear polarization at high magnetic field. Journal of biomolecular NMR 2014, 60 (2–3), 157–168. [PubMed: 25284462]

(9). Rankin AG; Trébosc J; Pourpoint F; Amoureux J-P; Lafon O Recent developments in MAS DNP-NMR of materials. Solid State Nucl. Magn. Reson 2019, 101, 116–143. [PubMed: 31189121]

(10). Biedenbänder T; Aladin V; Saeidpour S; Corzilius B. r. Dynamic Nuclear Polarization for Sensitivity Enhancement in Biomolecular Solid-State NMR. Chemical Reviews 2022, 122, 9738–9794. [PubMed: 35099939]

(11). Albert BJ; Gao C; Sesti EL; Saliba EP; Alaniva N; Scott FJ; Sigurdsson ST; Barnes AB Dynamic nuclear polarization nuclear magnetic resonance in human cells using fluorescent polarizing agents. Biochemistry 2018, 57 (31), 4741–4746. [PubMed: 29924582]

(12). Gao C; Alaniva N; Saliba EP; Sesti EL; Judge PT; Scott FJ; Halbritter T; Sigurdsson ST; Barnes AB Frequency-chirped dynamic nuclear polarization with magic angle spinning using a frequency-agile gyrotron. J. Magn. Reson 2019, 308, 106586. [PubMed: 31525550]

(13). Rosay M; Blank M; Engelke F Instrumentation for solid-state dynamic nuclear polarization with magic angle spinning NMR. J. Magn. Reson 2016, 264, 88–98. [PubMed: 26920834]

(14). Can T; Ni Q; Griffin R Mechanisms of dynamic nuclear polarization in insulating solids. J. Magn. Reson 2015, 253, 23–35. [PubMed: 25797002]

(15). Kundu K; Mentink-Vigier F; Feintuch A; Vega S In DNP mechanisms. Handbook of High Field Dynamic Nuclear Polarization; 2019; p 15

(16). Jeffries C Dynamic orientation of nuclei by forbidden transitions in paramagnetic resonance. Phys. Rev 1960, 117 (4), 1056.

(17). Schmugge T; Jeffries C High dynamic polarization of protons. Phys. Rev 1965, 138 (6A), A1785.

(18). Hwang CF; Hill DA Phenomenological model for the new effect in dynamic polarization. Phys. Rev. Lett 1967, 19 (18), 1011.

(19). Kessenikh A; Lushchikov V; Manenkov A; Taran YV Proton polarization in irradiated polyethylenes. Soviet Phys.-Solid State (English Transl.) 1963, 5, 321.

(20). Kessenikh A; Manenkov A; Pyatnitskii G On explanation of experimental data on dynamic polarization of protons in irradiated polyethylenes. Soviet Phys.-Solid State (English Transl.) 1964, 6, 641.

(21). de Boer W Dynamic orientation of nuclei at low temperatures. Journal of Low Temperature Physics 1976, 22 (1), 185–212.

(22). Borghini M Spin-temperature model of nuclear dynamic polarization using free radicals. Phys. Rev. Lett 1968, 20 (9), 419.

(23). Wenckebach WT Dynamic nuclear polarization via the cross effect and thermal mixing: A. The role of triple spin flips. J. Magn. Reson 2019, 299, 124–134. [PubMed: 30594883]

(24). Wenckebach WT Dynamic nuclear polarization via the cross effect and thermal mixing: B. Energy transport. J. Magn. Reson 2019, 299, 151–167. [PubMed: 30597441]

(25). Carver TR; Slichter CP Experimental verification of the Overhauser nuclear polarization effect. Phys. Rev 1956, 102 (4), 975.

(26). Corzilius B High-field dynamic nuclear polarization. Annu. Rev. Phys. Chem 2020, 71, 143–170. [PubMed: 32074473]

(27). Dementyev AE; Cory DG; Ramanathan C High-field Overhauser dynamic nuclear polarization in silicon below the metal-insulator transition. J. Chem. Phys 2011, 134 (15), 154511. [PubMed: 21513399]

(28). Järvinen J; Zvezdov D; Ahokas J; Sheludiakov S; Lehtonen L; Vasiliev S; Vlasenko L; Ishikawa Y; Fujii Y Dynamic nuclear polarization and ESR hole burning in As doped silicon. Phys. Chem. Chem. Phys 2020, 22 (18), 10227–10237. [PubMed: 32352086]

(29). Haze O; Corzilius B; Smith AA; Griffin RG; Swager TM Water-soluble narrow-line radicals for dynamic nuclear polarization. J. Am. Chem. Soc 2012, 134 (35), 14287–14290. [PubMed: 22917088]

(30). Can TV; Caporini MA; Mentink-Vigier F; Corzilius B; Walish JJ; Rosay M; Maas WE; Baldus M; Vega S; Swager TM; et al. Overhauser effects in insulating solids. J. Chem. Phys 2014, 141 (6), 064202. [PubMed: 25134564]

(31). Ji X; Can T; Mentink-Vigier F; Bornet A; Milani J; Vuichoud B; Caporini M; Griffin RG; Jannin S; Goldman M; et al. Overhauser effects in non-conducting solids at 1.2 K. J. Magn. Reson 2018, 286, 138–142. [PubMed: 29241045]

(32). Gurinov A; Sieland B; Kuzhelev A; Elgabarty H; Kühne TD; Prisner T; Paradies J; Baldus M; Ivanov KL; Pylaeva S Mixed-Valence Compounds as Polarizing Agents for Overhauser Dynamic Nuclear Polarization in Solids. Angew. Chem., Int. Ed 2021, 60 (28), 15371–15375.

(33). Perras FA; Flesariu DF; Southern SA; Nicolaides C; Bazak JD; Washton NM; Trypiniotis T; Constantinides CP; Koutentis PA Methyl-Driven Overhauser Dynamic Nuclear Polarization. J. Phys. Chem. Lett 2022, 13, 4000–4006. [PubMed: 35482607]

(34). Pylaeva S; Ivanov KL; Baldus M; Sebastiani D; Elgabarty H Molecular mechanism of Overhauser dynamic nuclear polarization in insulating solids. J. Phys. Chem. Lett 2017, 8 (10), 2137–2142. [PubMed: 28445055]

(35). Pylaeva S; Marx P; Singh G; Kühne TD; Roemelt M; Elgabarty H Organic Mixed-Valence Compounds and the Overhauser Effect in Insulating Solids. J. Phys. Chem. A 2021, 125 (3), 867–874. [PubMed: 33464904]

(36). Li Y; Equbal A; Tabassum T; Han S 1H thermal mixing dynamic nuclear polarization with BDPA as polarizing agents. J. Phys. Chem. Lett 2020, 11 (21), 9195–9202. [PubMed: 33058676]

(37). Delage-Laurin L; Palani RS; Golota N; Mardini M; Ouyang Y; Tan KO; Swager TM; Griffin RG Overhauser dynamic nuclear polarization with selectively deuterated BDPA radicals. J. Am. Chem. Soc 2021, 143 (48), 20281–20290. [PubMed: 34813311]

(38). Ong T-C; Mak-Jurkauskas ML; Walish JJ; Michaelis VK; Corzilius B. r.; Smith AA; Clausen AM; Cheetham JC; Swager TM; Griffin RG Solvent-free dynamic nuclear polarization of amorphous and crystalline ortho-terphenyl. J. Phys. Chem. B 2013, 117 (10), 3040–3046. [PubMed: 23421391]

(39). Chaudhari SR; Wisser D; Pinon AC; Berruyer P; Gajan D; Tordo P; Ouari O; Reiter C; Engelke F; Copéret C; et al. Dynamic nuclear polarization efficiency increased by very fast magic angle spinning. J. Am. Chem. Soc 2017, 139 (31), 10609–10612. [PubMed: 28692804]

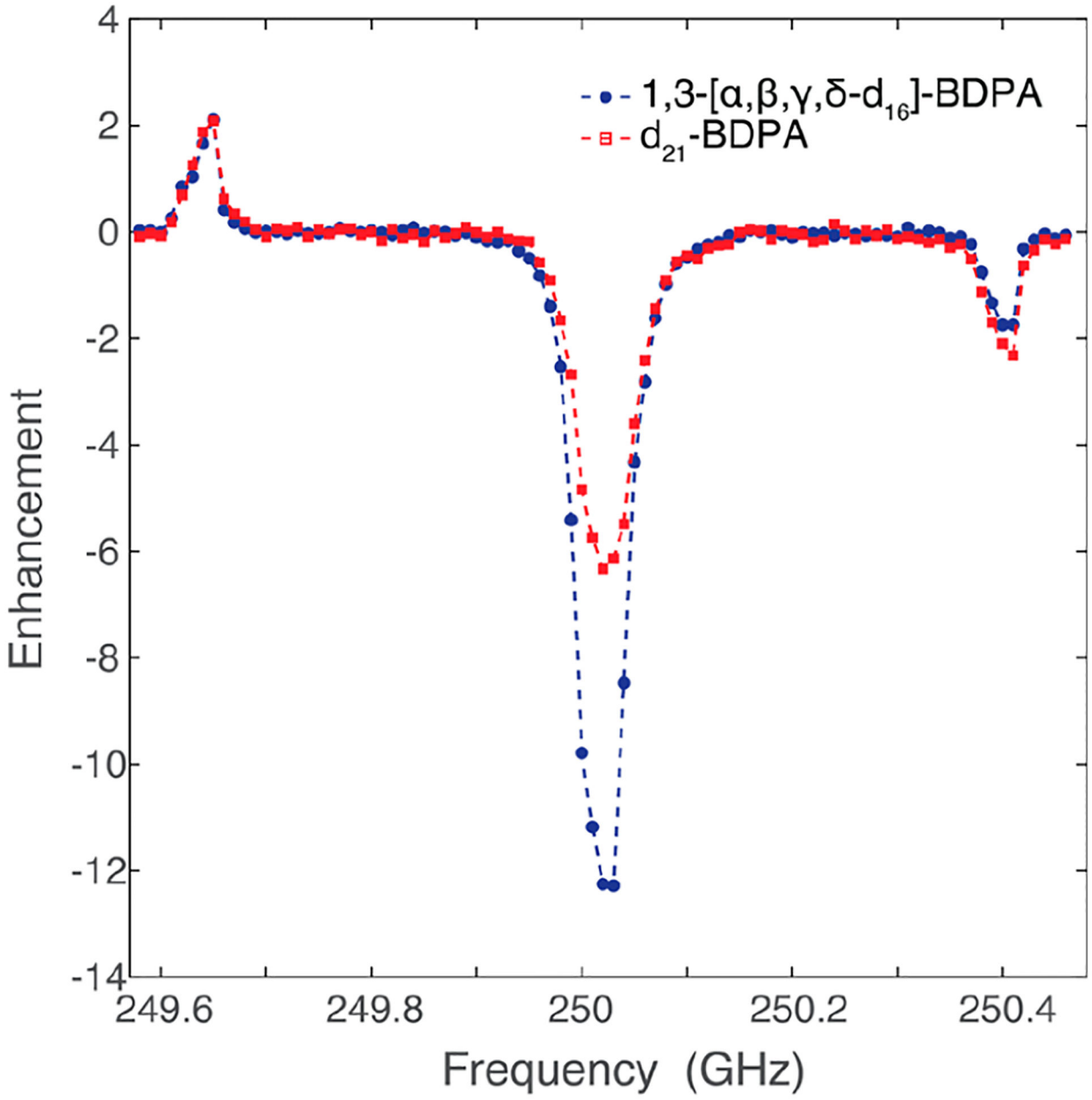

Figure 1.

DNP frequency profile obtained 8.9 T spectrometer on 1,3, [$\alpha,\beta,\gamma,\delta$-$d_{16}$]-BDPA (blue) and d_{21}-BDPA (red), both spinning at a MAS frequency of 5 kHz and at 90 K. The incident microwave power was 160 mW.

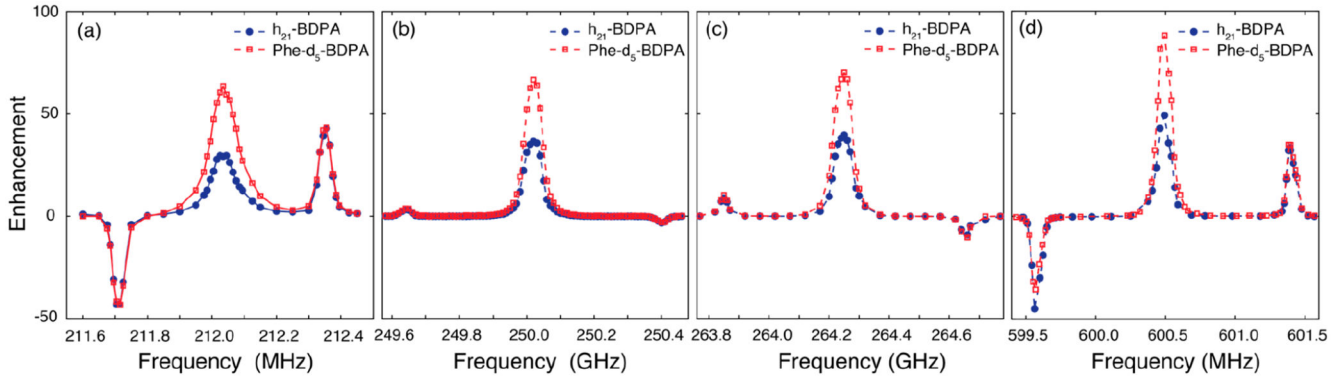

Figure 2.

(a) DNP field profile obtained at 5 T (b) DNP frequency profile obtained at 8.9 T with a 160 mW low-power microwave source, (c) DNP frequency profile at 9.4 T with a 280 mW low-power microwave source, and (d) DNP field profile at 14.1 T with a gyrotron for h_{21}-BDPA (blue) and Phe-d_5-BDPA (red). The data at 8.9 T was obtained at 90 K, while the data at 9.4 and 14.1 T were obtained at 100 K. The measurements were made on a sample spinning at a MAS frequency of 3.5 kHz (a) or 5 kHz (b–d).

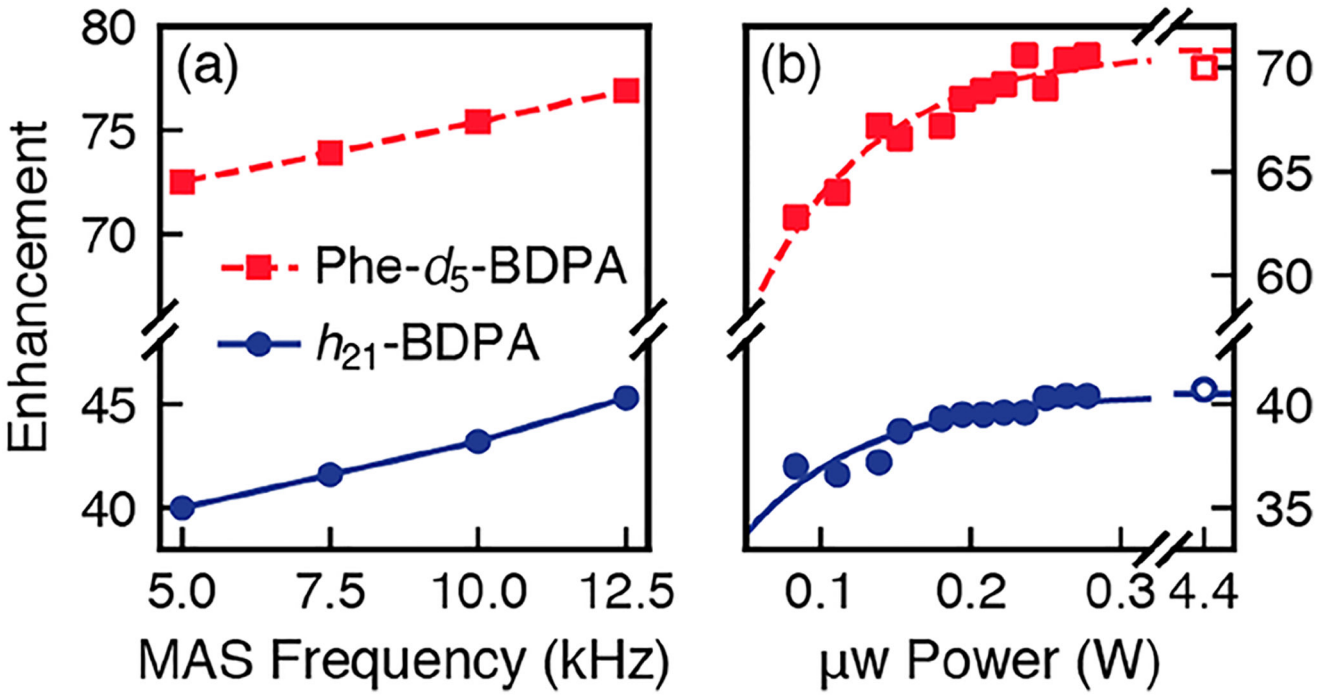

Figure 3.

Experimental ^{1}H DNP enhancements of h_{21}-BDPA and Phe-d_5-BDPA as a function of (A) MAS frequency and (B) incident microwave power obtained at the 9.4 T DNP spectrometer with a maximum power of 280 mW. The empty circle and square are data points obtained on the 8.9 T DNP spectrometer with an incident microwave power of 4.4 W from a gyrotron. The data in part a were obtained with an incident microwave power of 280 mW and the data in part b were obtained with a MAS frequency of 5 kHz.

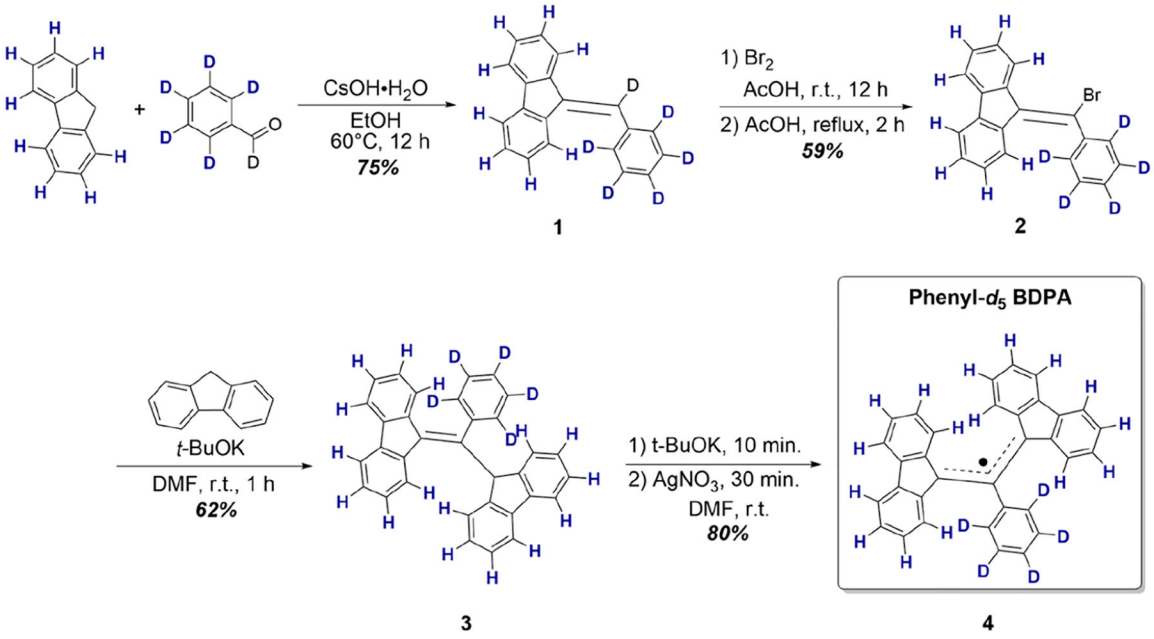

Scheme 1.
Synthetic Route to Phe-d_5-BDPA Radical

Table 1.

Experimentally Measured Spin–Lattice Relaxation Times (T_1) and DNP Buildup Times (T_B) for h_{21}-BDPA and Phe-d_5-BDPA at 8.9 T and 14.1 (DNP Spectrometers Described in the Text)

	h_{21}-BDPA		Phe-d_5-BDPA	
	T_1 (s)	T_B (s)	T_1 (s)	T_B (s)
8.9 T	32.1 ± 2.2	37.5 ± 1.5	38.0 ± 0.4	29.6 ± 0.3
14.1 T	31.9 ± 1.5	30.1 ± 1.5	37.1 ± 3.9	28.9 ± 2.0

Table 2.

Experimentally Measured OE DNP Enhancement for 2.5 wt % h_{21}-BDPA and Phe-d_5-BDPA at 5 T with a Gyrotron, at 8.9 T with both a Low-Power Microwave Source and a Gyrotron, at 9.4 T with a Low-Power Source, and 14.1 T with a Gyrotron[a]

	h_{21}-BDPA		Phe-d_5-BDPA
	measured	**adjusted**	**measured**
5 T/2 W	29.2	35.0	63.6
8.9 T/160 mW	36.5	43.8	66.6
8.9 T/4.4 W	40.7	48.8	70.0
9.4 T/280 mW	39.7	47.6	70.3
14.1 T/30 W	49.2	59.0	88.2

[a]The enhancement values adjusted for the concentration difference (1.0:1.2) as measured by UV–vis are listed for h_{21}-BDPA, normalized for Phe-d_5-BDPA